

Metabolomic response of osteosarcoma cells to nanographene oxide-mediated hyperthermia

Mónica Cicuéndez^{1,2,*}, Joana Flores¹, Helena Oliveira^{1,3}, M.Teresa Portolés⁴, María Vallet-Regí^{5,6}, Mercedes Vila^{2,+}, Iola F. Duarte^{1,*,+}

¹CICECO-Aveiro Institute of Materials, Department of Chemistry, University of Aveiro (UA), Aveiro, Portugal.

²NRG-TEMA, Department of Mechanical Engineering, University of Aveiro (UA), Portugal.

³CESAM, Department of Biology, University of Aveiro (UA), Aveiro, Portugal.

⁴Department of Biochemistry and Molecular Biology I, Faculty of Sciences Chemistry, University Universidad Complutense of Madrid, Instituto de Investigación Sanitaria del Hospital Clínico San Carlos (IdISSC), Ciudad Universitaria s/n, 28040-Madrid, Spain.

⁵Department of Inorganic and Bioinorganic Chemistry, Faculty of Pharmacy, University Complutense of Madrid, Instituto de Investigación Sanitaria Hospital 12 de Octubre i+12, Ciudad Universitaria s/n, 28040-Madrid, Spain.

⁶Networking Research Center on Bioengineering, Biomaterials and Nanomedicine, CIBER-BBN, Spain.

*corresponding authors: ioladuarte@ua.pt; mcicuendez@ua.pt.

⁺these authors contributed equally to this work.

ABSTRACT

Nanographene oxide (nGO)-mediated hyperthermia has been increasingly investigated as a localised, minimally invasive anticancer therapeutic approach. Near InfraRed (NIR) light irradiation for inducing hyperthermia is particularly attractive, because biological systems mostly lack chromophores that absorb in this spectral window, facilitating the selective heating and destruction of cells which have internalized the NIR absorbing-nanomaterials. However, little is known about biological effects accompanying nGO-mediated hyperthermia at cellular and molecular levels. In this work, well-characterised pegylated nGO sheets with a hydrodynamic size of 300 nm were incubated with human Saos-2 osteosarcoma cells for 24h and their incorporation verified by flow cytometry and confocal microscopy. No effect on cell viability was observed after nGO incorporation by Saos-2 cells. However, a proliferation delay was observed due to the presence of nGO sheets in the cytoplasm. ^1H NMR metabolomics was employed to screen for changes in the metabolic profile of cells, as this could help to improve understanding of cellular responses to nanomaterials and provide new endpoint markers of effect. Cells incorporating nGO sheets showed noticeable changes in 10 metabolites compared to control cells, including decreased levels of several amino acids, taurine and creatine and increased levels of phosphocholine and uridine/adenosine nucleotides. After NIR irradiation, cells showed decreases in glutamate and uridine nucleotides, together with increases in glycerophosphocholine and adenosine monophosphate. Overall, this study has shown that the cellular metabolome sensitively responded to nGO exposure and nGO-mediated hyperthermia and that NMR metabolomics is a powerful tool to investigate treatment responses.

Keywords: pegylated nanographene oxide (nGO) sheets, hyperthermia, cancer, Saos-2 osteoblasts, HRMAS ^1H NMR, metabolomics, cell metabolism.

Introduction

The development of alternative and/or complementary therapeutic strategies that can efficiently eliminate tumor cells without causing major deleterious side effects is a crucially important goal in the fight against cancer [1-6]. Tumor destruction through nanomaterial-mediated hyperthermia has been increasingly investigated as a minimally invasive alternative to surgery, as well as to treat tumors embedded in vital regions where surgical resection is not feasible [7,8]. In this type of therapy, an energy-absorbing nanosystem localized within tumor tissues absorbs energy provided by an external source and converts it into heat, thereby inducing localized thermal destruction (above 40°C) without affecting the surrounding tissues, which have not incorporated the nanomaterial [9-11]. The use of Near Infrared (NIR) light in the 700-1100 nm range for inducing tumor hyperthermia is particularly attractive, because biological systems mostly lack chromophores that absorb in this spectral window, facilitating the selective heating and destruction of cells which have internalized the NIR absorbing-nanomaterials [12-14].

Several nanomaterials are being developed for use in nanotechnology-based hyperthermia methods [15-20]. Nanosized graphene, particularly graphene oxide (nGO), represents one of the most thrilling candidates for this application, especially due to its strong NIR optical absorption ability [21-23]. Moreover, nGO has other fascinating properties which make it exquisitely suitable for nanomedicine applications, such as excellent aqueous processability, amphiphilicity, Surface Enhanced Raman Scattering (SERS) property, and fluorescence quenching ability [24].

Nanographene oxide-mediated hyperthermia has been studied *in vitro* [25-27] and *in vivo* [28,29]. It is known that depending on the laser fluency, different temperature increments and various thermodynamic and thermo-biological responses can occur in the

tissue medium [30]. However, there is still limited understanding of the biological effects accompanying nGO-mediated hyperthermia at the cellular and molecular levels. For instance, to our knowledge, no data concerning the metabolic changes produced in tumor cells by nGO-mediated hyperthermia have been described so far. The cellular metabolome (inventory of small molecules acting as substrates/products of enzyme-mediated reactions) closely reflects biochemical activity and functional status, being currently recognized as a key player in the cellular response to external stimuli such as nanomaterials[31,32]. Hence, the ability to comprehensively describe multiple metabolite changes (in a single analytical run) is expected to provide improved understanding of biological processes, compared to conventional single endpoint readouts.

In the present study, well-characterised pegylated nGO sheets (size of 300 nm) were incubated with human Saos-2 osteosarcoma cells for 24h and their internalization verified, along with the impact on cell viability and proliferation. Then, ¹H NMR analysis of lysed cell pellets was employed to assess the changes in the cellular metabolome induced by nGO incorporation and subsequent laser irradiation (1.5 W/cm² power, 5 min). This approach is expected to help improving current understanding of cellular responses to nGO-mediated hyperthermia and to provide potential endpoint markers of effect.

Materials and methods

Synthesis and characterization of pegylated nGO sheets

Pegylated nGO sheets have been obtained from exfoliation of high-purity graphite in an acidic medium by a modified Hummers method, as previously reported [33]. The resulting nGO suspension was dialyzed until pH 7, and activated with chloroacetic acid (Cl-CH₂-COOH) under strongly basic conditions (NaOH) to promote -COOH groups at

the surface. Then, it was functionalized by covalent bonding (diimide activation by adding EDAC:1-Ethyl-3-(3-dimethylaminopropyl) carbodiimide hydrochloride) with the non-toxic and non-immunogenic polymer Poly(Ethylene Glycolamine)(PEG) to improve colloidal stability and minimize immunogenicity. Finally, nGO sheets linked to PEG were marked with the amine reactive dye fluoresceinisothiocyanate (FITC) covalently bonded to the PEG. The resulting samples were analyzed by Atomic Force Microscopy AFM *multimode* Nanoscope III A (Bruker). Dynamic lightscattering (DLS) measurements were also performed in pH 5 solutions in a Zetasizer Nano series instrument equipped with a 633 nm “red” laser from Malvern Instruments, with reproducibility being verified by collection and comparison of sequential measurements. Z-average sizes of three sequential measurements were collected at room temperature (RT) and analyzed. X-Ray Photoelectron Spectroscopy (XPS) spectra were acquired in a Ultra High Vacuum (UHV) system with a base pressure of 2×10^{-10} mbar. nGO-PEG powder was dispersed in MQ H₂O and drop coated on a Si wafer. The system is equipped with a hemispherical electron energy analyzer (SPECS Phoibos 150), a delay-line detector and a monochromatic AlK α (1486.74 eV) X-ray source. High resolution spectra were recorded at normal emission take-off angle and with a pass-energy of 20 eV, which provides an overall instrumental peak broadening of 0.5 eV. The XPS spectra were calibrated in binding energy by referencing to the first component of the C 1s spectrum to 284.8 eV.

Cell culture for nGO incorporation and cell proliferation studies

Human Saos-2 osteoblasts were seeded at a density of 10^5 cells/mL in DMEM culture medium supplemented with 10% FBS, 1 mM L-glutamine, penicillin, streptomycin, under a 5% CO₂ atmosphere and at 37°C for 24h. After this time, 75 μ g/mL of nGO material

were added to the medium and the cells were cultured for 24h in contact with nGO solution. Then, the attached cells were harvested with 0.25% trypsin-EDTA and counted with a Neubauer hemocytometer, using trypan blue for assessing viability. For assessing nGO cellular incorporation, the fluorescence of nGO was excited at 488 nm and measured with a 530/30 band pass filter in a FACScalibur Becton Dickinson flow cytometer. The conditions for data acquisition and flow cytometric analysis were established using negative and positive controls with the CellQuest Program of Becton Dickinson and these conditions were maintained during all the experiments. Each experiment was carried out three times and single representative experiments are displayed. For statistical significance, at least 10^4 cells were analyzed in each sample and the mean of the fluorescence emitted by these single cells was used.

Confocal microscopy studies

Cells were seeded on glass coverslips and cultured in the presence of pegylated nGO material for 24h, fixed with 3.7% paraformaldehyde in PBS, permeabilized with 0.1% Triton X-100 and preincubated with PBS containing 1% BSA. Then, cells were incubated for 20 min with rhodamine-phalloidin (1:40), stained with 40-6-diamidino-20-phenylindole (DAPI, 3×10^{-6} M in PBS) and examined using a Leica SP2 Confocal Laser Scanning Microscope. Rhodamine fluorescence was excited at 540 nm and measured at 565 nm. DAPI fluorescence was excited at 405 nm and measured at 420-480 nm.

NIR laser irradiation

NIR radiation was provided by a high-power (30 W) diodelaser (LASING S.A.) emitting in 808 nm, giving a circular irradiation area of diameter 3 cm (fluency: 4 J cm⁻²). The module allows irradiation of culture plates in a sterile environment. Irradiation was performed after nGO–cell uptake which, based on previous results, was considered complete after 24 h of Saos-2 exposure to nGO solution. Laser irradiation was performed at 1.5 W/cm² power during 5 min, based on previously reported results [30]. Afterwards, cells were harvested using 0.25% trypsin–EDTA, washed with deuterated PBS (pH 7.4), centrifuged (1000g, 6 min, 4°C), re-suspended in 40 µL PBS/D₂O, and stored at -80°C until Nuclear Magnetic Resonance (NMR) analysis.

NMR analysis

Thawed cells were mechanically lysed by a three fold cycle of nitrogen freezing and sonication [34], and 50 µl of each sample were transferred into a High Resolution Magic Angle Spinning (HR-MAS) rotor. NMR spectra were acquired on a Bruker Avance DRX-500 spectrometer operating at 500.13 MHz for ¹H observation, at 277 K, using a 4 mm HRMAS probe, in which the rotor containing the sample was spun at 4 kHz. To attenuate broad signals of macromolecules and improve the detection of small metabolites, the T₂-edited Carr-Purcell-Meiboom-Gill spin-echo pulse sequence with water presaturation ('cpmgrp1d' in Bruker library) was employed, using a total spin echo time of 60 ms (n = 150, τ = 200 µs). Each 1D spectrum was acquired with 2048 transients, 32 k data points, a spectral width of 6510.42 Hz, a relaxation delay of 2 s, and an acquisition time of 2.5 s. Spectra were processed with a line broadening of 0.3 Hz and zero-filling factor of 2, manually phased and baseline corrected. Chemical shifts were referenced internally to the alanine signal at δ 1.48 ppm. Spectral assignment was based on 2D total correlation spectroscopy (TOCSY) and heteronuclear single quantum coherence (HSQC) spectra and

consultation of spectral databases, such as the Bruker Biorecode database and the human metabolome HMDB database [35].

Multivariate analysis and integration of NMR data

Data matrices of total area-normalized spectra were built in Amix-viewer (version 3.9.14, BrukerBiospin, Rheinstetten) and multivariate analysis (MVA) was performed in SIMCA-P11.5 (Umetrics, Sweden). Principal component analysis (PCA) was followed by partial least square discriminant analysis (PLS-DA), whereby a 7-fold internal cross-validation was applied to assess the explained variance (R^2) and predictive power (Q^2). The corresponding loadings were obtained by multiplying the loading weight (w) by the standard deviation of each variable, and were color-coded according to variable importance to the projection (VIP).

To assess the magnitude of metabolite variations, selected spectral peaks were integrated in Amix-viewer, and normalized by the total area of each spectrum (excluding the suppressed water signal). For each metabolite, the magnitude of variation in nGO-treated/laser irradiated samples relatively to controls was assessed by calculating the effect size (ES), adjusted for small sample numbers, and respective standard error, according to the equations provided in the literature [36]. The metabolic changes with absolute ES larger than 0.8 (and with standard error $<$ ES) were represented graphically and the two-sample t-test (95% confidence level) was used to assess statistical significance of variations.

Statistics

Data are expressed as means \pm standard deviations of a representative of three experiments carried out in triplicate. Statistical analysis was performed using the Statistical Package for the Social Sciences (SPSS) version 19 software. Statistical comparisons were made by analysis of variance (ANOVA). Scheffé test was used for *post hoc* evaluations of differences among groups. In all of the statistical evaluations, $p < 0.05$ was considered as statistically significant.

Results and discussion

Synthesis and characterization of pegylated nGO sheets

Nanographene oxide (nGO) sheets, successfully obtained by the modified Hummers' method, were characterized by AFM, XPS, zeta-potential (ζ) and DLS particle size analysis. The chemical exfoliation of graphite in aqueous media, followed by chemical activation and size separation by centrifugation, resulted in pegylated nGO sheets having an average thickness of around 9 nm, corresponding to 13-14 layers (**Figure 1A**). Moreover, these nGO sheets had a hydrodynamic size distribution in the 200-550 nm range, with the largest number of nanosheets presenting sizes around 300 nm, as shown by DLS data (**Figure 1B**). Pegylated nGO sheets were also characterized by XPS to study the elemental composition and chemical environment of the elements present within their surface. **Figure 1C** shows a fitted C 1s spectrum, composed by four components centered at: 284.8 eV (C-C/C=C), 286.3 eV (C-O/C-N), 287.7 eV (C=O) and 288.9 eV (O-C=O/N-C=O). In general, the treatment carried out to promote the carboxylation of GO from surface hydroxyl and epoxide groups diminishes the intensity of the peak of the C 1s spectrum associated to C-O groups (at 286.3 eV). Thus, the high intensity of this peak after the pegylation process indicates successful incorporation of PEG-diamine. Finally, zeta-potential analysis was carried out to evaluate the surface charge of the nGO sheets.

According to previously published data [37], the zeta-potential of chemically activated nGO sheets with -COOH surface groups is -37.8 ± 8 mV. After the pegylation process, the zeta-potential value changed slightly to -32 ± 6 mV, which confirms the existence of the positive amino ended branches.

Cell uptake of pegylated nGO sheets and cell proliferation studies

Incorporation of the pegylated nGO sheets and its effects on the proliferation and viability of human osteosarcoma Saos-2 cells were evaluated after 24h of incubation with $75 \mu\text{g/mL}$ of nGO. The internalization of pegylated nGO was confirmed by flow cytometry, after adding trypan blue to quench the fluorescence produced by the nGO adsorbed on the outer surface of cells (**Figure 2A**, orange fluorescence profile) [38]. As it can be observed, similar fluorescence profiles were obtained with and without trypan blue (orange and blue profiles, respectively), indicating that pegylated nGO sheets with 300 nm size and a surface charge of -32 mV were completely internalized by human Saos-2 osteoblasts after 24h of treatment. Confocal microscopy was additionally carried out to evaluate the Saos-2 morphology in the presence of pegylated nGO sheets and to study its intracellular localization. **Figure 2B** and **Figure 2C** show the human Saos-2 osteoblasts morphology after 24h of treatment without and with nGO sheets, respectively. The results highlight that these pegylated nGO sheets have been incorporated by Saos-2 osteoblasts and were dispersed throughout the cytoplasm, as indicated by arrows. These results are in agreement with those published by other authors, where most of the GO that entered cells distributed in the cytoplasm with very few particles being present in the nucleus [39,40]. As for the uptake mechanism, although this was not assessed in the present study, it has been previously reported that Saos-2 cells take up these pegylated nGO sheets mainly by macropinocytosis, although microtubule-dependent pathways may also be

involved [41]. Moreover, Chartterjee and co-workers demonstrated that GO enters the cell through clathrin-mediated endocytosis as well as macropinocytosis [42].

The results obtained for viability and proliferation of human Saos-2 osteoblasts upon 24h nGO treatment are shown in **Figure 3**. High percentages of viability were obtained in all experimental conditions (97 and 93% in control and nGO-treated cells, respectively) and no significant differences were observed (**Figure 3A**). With respect to the effect of nGO treatment on Saos proliferation (**Figure 3B**), a significant delay in cell proliferation was observed, which is in agreement with previous results [43]. The high cell viability observed for nGO-exposed cells indicates that the plasma membrane integrity was highly preserved during the nano-bio interaction and subsequent nGO internalization by Saos-2 cells. This is in contrast with other studies where graphene and graphene-based nanomaterials were shown to alter the dynamics and integrity of the plasma membrane during their internalization, inducing cell death [44]. Some authors suggested that the serious membrane disruption could be attributed to the strong electrostatic interactions between the graphene surface and the lipid bilayer of the cell membrane [45]. Others revealed that certain types of graphene, such as pristine graphene, could impair cell membrane integrity by regulation of membrane- and cytoskeleton-associated genes [46]. In the present study, the absence of membrane damage is likely due to surface functionalization of the nGO sheets by the non-toxic and non-immunogenic polymer PEG [47].

As for the proliferation delay observed after nGO internalization (**Figure 3B**), the results are in agreement with those published by other authors, where a cytotoxicity evaluation of graphene oxide on different cells types was carried out [48-50]. The possible mechanism involved in the Saos-2 osteoblasts proliferation delay could be related to mitogen-activated protein kinases (MAPKs). It is well established that such kinases are

involved in the regulation of cell growth, proliferation, migration and apoptosis [51]. Matesanz and co-workers reported that nGO sheets were localized on F-actin filaments of Saos-2 osteoblasts after their internalization, and thus altered cell cycle in a cytoskeleton-dependent manner [43]. Moreover, Tian X, *et al* have recently published that nGO sheets retard cellular migration via disruption of actin cytoskeleton [52]. Therefore, considering that proliferation is dependent on the cell-cycle progress, it may be suggested that the uptake of our graphene oxide nanosheets could induce cell-cycle alterations, which would cause the proliferation delay observed.

Metabolic response to nGO incorporation and NIR laser irradiation

The metabolic composition of human Saos-2 osteosarcoma cells was assessed by HRMAS ¹H NMR analysis of lysed cell pellets. A representative cell spectrum is shown in **Figure 4**. Similarly to what has been reported for other tumor cell lines [53-56], the signals of several amino acids (e.g. alanine, glutamate, glycine), reduced glutathione (GSH), lactate, creatine, choline-containing compounds, taurine, myo-inositol and uridine/adenosine nucleotides could be unambiguously identified. Phosphocholine was one of the most abundant metabolites detected, likely reflecting the high malignancy of the Saos-2 cell line, since this metabolite is considered a biomarker of tumor malignant transformation [57]. Other metabolites closely related to tumor progression, such as choline and creatine (reported to be inversely expressed in later stages of tumor growth), were also clearly detected. On the other hand, glucose was absent from the Saos-2 metabolic profile, in agreement with the composition reported for osteosarcoma [58] and other tumor cell lines [53]. In non-tumor cells, the glucose flux through the glycolytic pathway is regulated to maintain a constant concentration of adenosine triphosphate (ATP). By contrast, glucose uptake and glycolysis are known to occur nearly 10 times faster in most

solid tumors compared with normal tissues [59], explaining the absence of this important metabolite in tumor cells.

To assess the impact of nGO incorporation and laser irradiation on the metabolic profile of Saos-2 cells, multivariate analysis was applied to the spectra collected for the three sample groups, *i.e.* controls cells, nGO-exposed cells (nGO) and nGO-exposed and laser irradiated cells (nGO+laser). The resulting PCA scores scatter plot (**Figure 5A**) showed that control and nGO-exposed cells were reasonably clustered and separated from each other (along the PC2 axis), while the laser-irradiated samples were more scattered, reflecting higher intra-group variability. Still, by applying PLS-DA, it was possible to discriminate the three sample groups along LV1 and LV2 axes (**Figure 5B**) and to highlight the main metabolites accounting for such discrimination based on the corresponding loadings profiles (**Figures 5C and 5D**). According to these profiles, nGO samples differed from controls in the levels of uridine nucleotides, alanine, glutamine, glycine, taurine and creatine (**Figure 5C**), while laser-irradiated samples were discriminated based on higher levels of glycerophosphocholine and AMP, together with lower levels of creatine and glutamate (**Figure 5D**). Spectral integration of individual metabolite signals was then carried out to assess the magnitude and statistical significance of the variations highlighted through multivariate analysis. The most relevant changes (absolute effect size > 0.8, as justified in ref 36) are summarized in **Figure 6**. In comparison to control cells, Saos-2 cells exposed to nGO showed consistent alterations in 10 metabolites (first column of the heatmap shown in **Figure 6**), namely decreases in taurine (-44%), glutamine (-35%), alanine (-34%), creatine (-33%), glycine (-26%), methionine (-25%) and glutamate (-15%), together with increases in phosphocholine (+24%), uridine nucleotides (+44%) and AMP (+59%). As for the effects of laser irradiation, compared to nGO-exposed cells, cells irradiated after nGO incorporation

showed higher levels of glycerophosphocholine (+38%) and AMP (+82%), together with decreased levels of glutamate (-34%) and uridine nucleotides (-20%) (second column of the heatmap shown in **Figure 6**).

One of the main metabolic alterations displayed by Saos-2 cells upon nGO incorporation and subsequent laser irradiation was a cumulative increase in the levels of AMP, suggesting that cellular energetic homeostasis was affected. The impact of graphene on mitochondrial function and energy production has been previously reported for other cell types [60-62]. For instance, in liver HepG2 cells, nGO sheets (400 nm) were reported to cause dysregulation of mitochondrial Ca^{2+} homeostasis and a decrease in mitochondrial membrane potential (MMP), which is crucial for ATP synthesis[60]. In another work, pegylatednGO sheets in the 100-200 nm size range were shown to interact with the mitochondria of MDA-MB-231 breast tumor cells and to reduce ATP generation, possibly in relation with the down-regulation of enzymes involved in the TCA cycle and oxidative phosphorylation [61]. Moreover, in mouse alveolar macrophages, GO has been proposed to participate in redox reactions with components of the mitochondrial electron transport chain, thereby leading to impairment of ATP production [62]. In the present study, ATP was not clearly detected in the ^1H NMR spectra, possibly due its rapid turnover. Still, the observed accumulation of AMP could be an indirect indication of energy shortage, reflecting the attempt of adenylate kinase to rescue ATP from ADP, with the concomitant production of AMP. In turn, a high level of AMP is recognized as an efficient activator of the AMP-activated protein kinase (AMPK), which is a crucial sensor of cellular energy status [63].

Upon activation, AMPK acts to restore energy homeostasis by stimulating catabolic reactions, while inhibiting ATP-consuming anabolic processes [63]. Interestingly, in the present study, the metabolic response to nGO comprised a consistent

decrease in the levels of several amino acids, all of which could be used as anaplerotic substrates for the tricarboxylic acid (TCA) cycle, presumably to increase energy production. Upon laser irradiation, nGO-exposed cells further decreased their glutamate levels, while the other amino acids levels (alanine, glutamine, methionine) remained similar to non-irradiated nGO-exposed cells. Moreover, nGO-incorporating cells showed decreased levels of creatine (synthesized from arginine and glycine), which could also relate to the impact of nGO on amino acid metabolism. On the other hand, phosphocholine registered a relevant increase in nGO-incorporating cells in relation to controls. As phosphocholine is central to the synthesis of the major cell membrane component phosphatidylcholine, its increment may reflect the down-regulation of phospholipid synthesis, in consonance with the putative AMPK-mediated inhibition of anabolic processes. This also agrees with the proliferation delay displayed by nGO-exposed Saos-2 cells (**Figure 3B**). Altogether, the metabolic variations described above suggest that AMPK activation may be an important player in the cellular responses to nGO and nGO-mediated hyperthermia, an hypothesis which needs to be verified in further studies.

Laser-irradiated cells further showed an increase in glycerophosphocholine, a well-known membrane breakdown product, likely reflecting heat-induced membrane damage [64]. Indeed, previous results demonstrated that nGO mediated hyperthermia under similar conditions to those applied in this study (low power and 7 min of laser exposure) caused Saos-2 osteoblasts death by mixed apoptotic/necrotic process, implying loss of the plasma membrane integrity [30]. Notably, glycerophosphocholine levels did not vary upon nGO incorporation in the absence of laser treatment, in agreement with the preservation of membrane integrity in non-irradiated nGO-incorporating cells (**Figure 3A**).

As taurine is an antioxidant metabolite [65], its decrease upon nGO incorporation could be related to nanomaterial-induced oxidative stress. However, while the generation of reactive oxygen species (ROS) has been reported to be a common response to graphene-based nanomaterials[40,42], previous results from our group have shown that pegylated nGO sheets of similar size did not increase ROS in Saos-2 cells [43]. Moreover, glutathione, another important antioxidant metabolite clearly detected in the cells profile, did not vary upon nGO incorporation, corroborating the absence of a strong oxidative stress response. Therefore, taurine variation likely relates to other possible roles of this metabolite, such as in osmoregulation, membrane stabilization, calcium homeostasis or protein phosphorylation [66].

Finally, nGO-incorporating cells showed increased levels of uridine nucleotides, which subsequently decreased after laser irradiation. The bioavailability of uridine is particularly crucial to the synthesis of RNA and biomembranes (via the formation of pyrimidine nucleotide–lipid conjugates), being also needed for the formation of UDP-sugar conjugates involved in the post-translational modification of proteins [67]. Therefore, the observed variations may possibly relate to the effects of nGO and hyperthermia on cell proliferation and/or protein glycosylation.

Conclusions

In this work, Saos-2 osteosarcoma cells were shown to incorporate 300 nm pegylated nGO sheets without impairing cell viability, while causing a delay in cell proliferation. These results were in agreement with other studies where nGO was found to distribute in the cells cytoplasm [39,40] and to interfere with cell cycle and growth [43]. At the metabolic level, nGO produced consistent variations in 10 metabolites, mainly reflecting changes in energy homeostasis, also seen in previous studies using other cell types and

different assays to assess mitochondrial function and energy production [61-63]. In particular, based on increased levels of AMP and phosphocholine, together with decreases in several amino acids, it has been newly hypothesized that AMPK activation may be an important player in the cellular responses to nGO. This hypothesis should be verified in future studies, as it could provide improved mechanistic understanding of nGO mode of action at the molecular level. Notably, subsequent laser irradiation of nGO-incorporating cells produced fewer effects: changes in AMP and glutamate were amplified, the levels uridine nucleotides recovered and glycerophosphoholine increased, this latter change likely reflecting laser-induced membrane damage, thus agreeing with previous results [30]. Membrane integrity was, however, not affected upon nGO incorporation, unlike the results reported by others where non-pegylated nGO was employed [45,46]. Overall, this study has shown that cellular metabolome sensitively responded to nGO exposure and nGO-mediated hyperthermia, and that NMR metabolomics is a powerful tool in nanotoxicity studies, allowing for new hypotheses on molecular mechanisms underlying treatment responses to be generated.

Acknowledgements

This work was developed within the scope of the project CICECO-Aveiro Institute of Materials, POCI-01-0145-FEDER-007679 (FCT Ref. UID /CTM /50011/2013), financed by national funds through the FCT/MEC and when appropriate co-financed by FEDER under the PT2020 Partnership Agreement. M.C. acknowledges the FCT financial support [Post-Doctoral Grant SFRH/BPD/101468/2014] and Operational Program Human Capital (POCH), European Union. H.O. acknowledges financial support FCT SFRH/BPD/111736/2015. M.T.P. acknowledges funding from Ministerio de Economía y Competitividad (projects MAT2013-43299-R and MAT2016-75611-R AEI/FEDER, UE). M.V.R. acknowledges funding from the European

Research Council (Advanced Grant VERDI; ERC-2015-AdG Proposal No. 694160). I.F.D. acknowledges the FCT/MCTES for a research contract under the Program ‘Investigador FCT’ 2014. The Portuguese National NMR Network supported with FCT funds and Bruker BioSpin GmbH for database access are also acknowledged. Thanks also to the staff of the Centro de Citometría y Microscopía de Fluorescencia of the Universidad Complutense de Madrid (Spain) and ICTS Centro Nacional de Microscopia Electrónica (Spain) for the assistance in the flow cytometry, confocal microscopy and AFM studies, respectively.

References

- [1] Sumer B, Gao J. Theranostic nanomedicine for cancer. *Nanomedicine***3**, 137-140 (2008).
- [2] Li L, Tang F, Liu H, Liu T, Hao N, Chen D, Teng X, He J. *In vivo* delivery of silica nanorattle encapsulated docetaxel for liver cancer therapy with low toxicity and high efficacy. *ACS Nano***4**, 6874-6882 (2010).
- [3] Zhang Z, Wang L, Wang J, Jiang X, Li X, Hu Z, Ji Y, Wu X, Chen C. Mesoporous silica-coated gold nanorods as a light-mediated multifunctional theranostic platform for cancer treatment. *Adv. Mater.* **24**, 1418-1423 (2012).
- [4] Liu Y, Ai K, Liu J, Deng M, He Y, Lu L. Dopamine-melanin colloidal nanospheres: an efficient near-infrared photothermal therapeutic agent for *in vivo* cancer therapy. *Adv. Mater.* **25**, 1353–1359 (2013).
- [5] Cheng L, Wang C, Feng L, Yang K, Liu, Z. Functional nanomaterials for phototherapies of cancer. *Chem. Rev.* **114**, 10869–10939 (2014).
- [6] Yang Yu, Jingjing L, Xiaoqi S, Liangzhu F, Wenwen Z, Zhuang L, Meiwang C. Near-infrared light-activated cancer cell targeting and drug delivery with aptamer-modified nanostructures. *Nano Research***9**, 139-148 (2016).
- [7] Beik J, Abed Z, Ghoreishi FS, Hosseini-Nami S, Mehrzadi S, Shakeri-Zadeh A, Kamrava SK. Nanotechnology in hyperthermia cancer therapy: From fundamental principles to advanced applications. *J. Controlled Release***235**, 205–221 (2016).
- [8] Fiorentini G, Szasz A. Hyperthermia today: electric energy, a new opportunity in cancer treatment. *J. Cancer Res. Ther.* **2**, 41-46 (2006).
- [9] Van de Broek B, Devoogdt N, D'Hollander A, Gijs HL, Jans K, Lagae L, Muyldermans S, Maes G, Borghs G. Specific cell targeting with nanobody conjugated branched gold nanoparticles for photothermal therapy. *ACS Nano***5**, 4319-4328 (2011).

- [10] Li-Sen L, Zhong-Xiao C, Jian-Bo C, Kai-Mei K, Qiao-Li P, Jinhao G, Huang-Hao Y, Gang L, Xiaoyuan C. Multifunctional Fe₃O₄@ polydopamine core-shell nanocomposites for intracellular mRNA detection and imaging-guided photothermal therapy. *ACS Nano***8**, 3876-3883 (2014).
- [11] Kossatz S, Grandke J, Couleaud P, Latorre A, Aire A, Crosbie-Staunton K, Ludwig R, Dähring H, Ettelt V, Lazaro-Carrillo A, Calero M, Sader M, Courty J, Volkov Y, Prina-Mello A, Villanueva A, Somoza Á, Cortajarena AL, Miranda R, Hilger I. Efficient treatment of breast cancer xenografts with multifunctionalized iron oxide nanoparticles combining magnetic hyperthermia and anti-cancer drug delivery. *Breast Cancer Res.* **17**, 1–17(2015).
- [12] Zhang Z, Wang J, Chen C. Near infrared light mediated nanoplatforms for cancer thermo-chemotherapy and optical imaging. *Adv. Mater.* **25**, 3869-3880 (2013).
- [13] Zhou J, Lu Z, Zhu X, Wang X, Liao Y, Ma Z, Li F. NIR photothermal therapy using polyaniline nanoparticles. *Biomaterials***34**, 9584-9592 (2013).
- [14] Yang K, *et al.* *In vitro* and *in vivo* near infrared photothermal therapy of cancer using polypyrrole organic nanoparticles. *Adv. Mater.***24**, 5586-5592 (2012).
- [15] Chen J, Glaus C, Laforest R, Zhang Q, Yang M, Gidding M, Welch MJ, Xia Y. Gold nanocages as photothermal transducers for cancer treatment. *Small***6**, 811-817 (2010).
- [16] Huiyu L, Dong C, Linlin L, Tianlong L, Longfei T, Xiaoli W, Fanggiong T. Multifunctional gold nanoshells on silica nanorattles: a platform for the combination of photothermal therapy and chemotherapy with low systemic toxicity. *Angew. Chem.***123**, 921-925 (2011).
- [17] Zha Z, Yue X, Ren Q, Dai Z. Uniform polypyrrole nanoparticles with high photothermal conversion efficiency for photothermal ablation of cancer cells. *Adv. Mater.***25**, 777-782 (2013).

- [18] Li Y, Lu W, Huang Q, Li C, Chen W. Copper sulfide nanoparticles for photothermal ablation of tumor cells. *Nanomedicine* **5**, 1161-1171 (2010).
- [19] Chou SS, Kaehr B, Kim J, Foley BM, De M, Hopkins PE, Huang J, Brinker CJ, Dravid VP. Chemically exfoliated MoS₂ as near-infrared photothermal agents. *Angew. Chem.* **125**, 4254-4258 (2013).
- [20] Qin L, Chunyang S, Qun H, Daobin L, Adnan K, Ting X, Ziyu W, Jun W, Li S. Ultrathin carbon layer coated MoO₂ nanoparticles for high-performance near-infrared photothermal cancer therapy. *Chem. Commun.* **51**, 10054-10057 (2015).
- [21] Tian B, Wang C, Zhang S, Feng L, Liu Z. Photothermally enhanced photodynamic therapy delivered by nano-graphene oxide. *ACS Nano* **5**, 7000-7009 (2011).
- [22] Miao W, Shim G, Lee S, Choe YS, Oh YK. Safety and tumor tissue accumulation of pegylated graphene oxide nanosheets for co-delivery of anticancer drug and photosensitizer. *Biomaterials* **34**, 3402-3410 (2013).
- [23] Sheng Z, Song L, Zheng J, Hu D, He M, Zheng M, Gao G, Gong P, Zhang P, Ma Y, Cai L. Protein-assisted fabrication of nano-reduced graphene oxide for combined *in vivo* photoacoustic imaging and photothermal therapy. *Biomaterials* **34**, 5236-5243 (2013).
- [24] Yanwu Z, Shanthi M, Weiwei C, Xuesong L, Ji Won S, Jeffrey R. P, Rodney S. R. Graphene and graphene oxide: Synthesis, Properties, and Applications. *Adv. Mater.* **22**, 3906-3924 (2010).
- [25] Robinson JT, Tabakman SM, Liang Y, Wang H, Sanchez Casalongue H, Vinh D, Dai H. Ultrasmall reduced graphene oxide with high near-infrared absorbance for photothermal therapy. *J. Am. Chem. Soc.* **133**, 6825-6831 (2011).
- [26] Yinghui Wang, Hengguo Wang, Dapeng Liu, Shuyan Song, Xiao Wang, Hongjie Zhang. Graphene oxide covalently grafted upconversion nanoparticles for combined NIR

mediated imaging and photothermal/photodynamic cancer therapy. *Biomaterials***34**, 7715-7724(2013).

[27] Zoran M. Markovic, Ljubica M. Harhaji-Trajkovic, Biljana M. Todorovic-Markovic, Dejan P. Kepic, Katarina M. Arsikin, Svetlana P. Jovanovic, Aleksandar C. Pantovic, Miroslav D. Dramicanin, Vladimir S. Trajkovic. *In vitro* comparison of the photothermal anticancer activity of graphene nanoparticles and carbon nanotubes. *Biomaterials***32**, 1121-1129(2011).

[28] Zhang H, Wu H, Wang J, Yang Y, Wu D, Zhang Y, Zhang Y, Zhou Z, Yang S. Graphene oxide-BaGdF₅ nanocomposites for multi-modal imaging and photothermal therapy. *Biomaterials***42**, 66–77 (2015).

[29] Jianbo C, Hengqing A, Xinglu H, Guifeng F, Rongqiang Z, Lei Z, Jin Xie, Fan Zhang. Monitoring of the tumor response to nano-graphene oxide-mediated photothermal/photodynamic therapy by diffusion-weighted and BOLD MRI. *Nanoscale***8**, 10152 (2016).

[30] Vila M, Matesanz MC, Gonçalves G, Feito MJ, Linares J, Marques PAAP, Portolés MT, Vallet-Regí M. Triggering cell death by nanographene oxide mediated hyperthermia. *Nanotechnology* **25**, 035101 (7pp)(2014).

[31] Shim W, Paik M. J, Duc-Toan N, Lee J-K, Lee Y, Kim J H, Shin E.-H, Kang J. S, Jung H.-S, Choi S, Park S, Shim J. S. Lee, G. Analysis of changes in gene expression and metabolic profiles induced by silica-coated magnetic nanoparticles. *ACS Nano***6**, 7665–7680 (2012).

[32] Xiangang H, Shaohu O, Li M, Jing A, Qixing Z. Effects of Graphene Oxide and Oxidized Carbon Nanotubes on the Cellular Division, Microstructure, Uptake, Oxidative Stress, and Metabolic Profiles. *Environ. Sci. Technol.* **49**, 10825–10833 (2015).

- [33] Gonçalves G, Marques P A A P, Granadeiro C, Nogueira H I S, Singh M K, Grácio J. Surface modification of graphene nanosheets with gold nanoparticles: the role of oxygen moieties at graphene surface on gold nucleation and growth. *Chem. Mater.* **21**, 4796–4802 (2009).
- [34] Duarte IF, Marques J, Ladeirinha AF, Rocha CM, Lamego I, Calheiros R, Silva TM, Marques MPM, Melo JB, Carreira IM, Gil AM. Analytical approaches towards successful human cell metabolome studies by NMR spectroscopy. *Anal. Chem.* **81**, 5023-5032 (2009).
- [35] Wishart DS, Jewison T, Guo AC, Wilson M, Knox C, Liu Y, Djoumbou Y, Mandal R, Aziat F, Dong E, Bouatra S, Sinelnikov I, Arndt D, Xia J, Liu P, Yallou F, Bjorn Dahl T, Perez-Pineiro R, Eisner R, Allen F, Neveu V, Greiner R, Scalbert A. HMDB 3.0 - The human metabolome database in 2013. *Nucleic Acids Res.* **41**, D801-D807 (2013).
- [36] Berben L, Sereika SM, Engberg S. Effect size estimation: methods and examples. *Int. J. Nurs. Stud.* **49**, 1039-1047 (2012).
- [37] Vila M, Portolés MT, Marques PAAP, Feito MJ, Matesanz MC, Ramírez-Santillán C, Gonçalves G, Cruz SMA, Nieto A, Vallet-Regí M. Cell uptake survey of pegylated nanographene oxide. *Nanotechnology* **23**, 465103 (9pp) (2012).
- [38] Busch W, Bastian S, Trahorsch U, Iwe M, Kühnel D, Meißner T, Springer A, Gelinsky M, Richter V, Ikonomidou C, Potthoff A, Lehmann I, Schirmer K. Internalisation of engineered nanoparticles into mammalian cells *in vitro*: Influence of cell type and particle properties. *J. Nanopart. Res.* **13** 293–310 (2010).
- [39] Kan Wang , Jing Ruan , Hua Song , Jiali Zhang , Yan Wo , Shouwu Guo , Daxiang Cui . Biocompatibility of graphene oxide. *Nanoscale Res. Lett.* **6**, 8(2010).

- [40] Zhang B, Wei P, Zhou Z, Wei T. Interactions of graphene with mammalian cells: Molecular mechanisms and biomedical insights. *Adv. Drug Deliv. Rev.* **105**, 145–162 (2016).
- [41] Linares J, Matesanz MC, Vila M, Feito MJ, Gonçalves G, Vallet-Regí M, Marques PAAP, Portolés MT. Endocytic mechanisms of graphene oxide nanosheets in osteoblasts, hepatocytes and macrophages. *ACS Appl. Mater. Interfaces* **6**, 13697–13706 (2014).
- [42] Chatterjee N, Eom H-J, Choi J. A systems toxicology approach to the surface functionality control of graphene-cell interactions. *Biomaterials* **35**, 1109-1127(2014).
- [43] Matesanz MC, Vila M, Feito MJ, Linares J, Gonçalves G, Vallet-Regí M, Marques PAAP, Portolés MT. The effects of graphene oxide nanosheets localized on F-actin filaments on cell-cycle alterations. *Biomaterials* **34**, 1562-1569(2013).
- [44] Syama S, Mohanan P.V. Safety and biocompatibility of graphene: A new generation nanomaterial for biomedical application. *Int. J. Biol. Macromolec.* **86**, 546–555 (2016).
- [45] Liao K.H, Lin Y.S, Macosko C.W, Haynes C.L. Cytotoxicity of graphene oxide and graphene in human erythrocytes and skin fibroblasts. *ACS Appl. Mater. Interfaces* **3**, 2607–2615 (2011).
- [46] Xu M, Zhu J, Wang F, Xiong Y, Wu Y, Wang Q, Weng J, Zhang Z, Chen W, Liu S. Improved in vitro and in vivo biocompatibility of graphene oxide through surface modification: poly(acrylic acid)-functionalization is superior to PEGylation. *ACS Nano* **10**, 3267–3281 (2016).
- [47] Shi R. Polyethylene glycol repairs membrane damage and enhances functional recovery: a tissue engineering approach to spinal cord injury. *Neurosci Bull*, **29**, 460–466 (2013).
- [48] Talukdar Y, Rashkow J.T, Lalwani G, Kanakia S, Sitharaman B. The effects of graphene nanostructures on mesenchymal stem cells. *Biomaterials* **35**, 4863–4877(2014).

- [49] Horváth L, Magrez A, Burghard M, Kern K, Forró L, Schwaller B. Evaluation of the toxicity of graphene derivatives on cells of the lung luminal surface. *Carbon***64**, 45–60 (2013).
- [50] Chang Y, Yang ST, Liu JH, Dong E, Wang Y, Cao A, Liu Y, Wang H. In vitro toxicity evaluation of graphene oxide on A549 cells. *Toxicol. Lett.***200**, 201–210 (2011).
- [51] Boutros T, Chevet E, Metrakos P. Mitogen-activated protein (MAP) kinase/MAP kinase phosphatase regulation: roles in cell growth, death, and cancer. *Pharmacol Rev.* **60**, 261- 310 (2008).
- [52] Tian X, Yang Z, Duan G, Wu A, Gu Z, Zhang L, Chen C, Chai Z, Ge C, Zhou R. Graphene oxide nanosheets retard cellular migration via disruption of actin cytoskeleton. *Small***13**, 1602133 (2017).
- [53] Maria RM, Altei WF, Andricopulo AD, Becceneri AB , Cominetti MR , Venâncio T , Colnago LA. Characterization of metabolic profile of intact non-tumor and tumor breast cells by high-resolution magic angle spinning nuclear magnetic resonance spectroscopy. *Anal. Biochem.***488**, 14-18 (2015).
- [54] Fedele TA, Galdos-Riveros AC, de Farias e Melo HJ, Magalhães A, Durvanei Augusto Maria. Prognostic relationship of metabolic profile obtained of melanoma B16F10. *Biomed Pharmacother***67**, 146–156(2013).
- [55] Bayet-Robert M, Loiseau D, Rio P, Demidem A, Barthomeuf C, Stepien G, Morvan D. Quantitative Two-Dimensional HRMAS ¹H-NMR Spectroscopy-Based Metabolite Profiling of Human Cancer Cell Lines and Response to Chemotherapy. *Magn. Reson. Med.***63**, 1172–1183 (2010).
- [56] da Silva AF, Sartori D, Macedo FC, Ribeiro LR, Fungaro MHP, Mantovani MS. Effects of β-glucan extracted from *Agaricus blazei* on the expression of ERCC5, CASP9,

and CYP1A1 genes and metabolic profile in HepG2 cells. *Hum. Exp. Toxicol***32**, 647–654 (2013).

[57] Eliyahu G, Kreizman T, Degani H. Phosphocholine as a biomarker of breast cancer: molecular and biochemical studies. *Int. J. Cancer***120**, 1721-1730 (2007).

[58] Duarte IF, Lamego I, Marques J, Marques MP, Blaise BJ, Gil AM. Nuclear magnetic resonance (NMR) study of the effect of cisplatin on the metabolic profile of MG-63 osteosarcoma cells. *J. Proteome Res.***9**, 5877-5886 (2010).

[59] Nelson DL, Cox MM. *Lehninger Principles of Biochemistry*. W. H. Freeman, San Francisco, 2008.

[60] Lammel T, Boisseaux P, Fernandez-Cruz ML, Navas JM, Internalization and cytotoxicity of graphene oxide and carboxyl graphene nanoplatelets in the human hepatocellular carcinoma cell line Hep G2. *Part. Fibre. Toxicol.***10**, 21pp (2013).

[61] Zhou H, Zhang B, Zheng J, Yu M, Zhou T, Zhao K, Jia Y, Gao X, Chen C, Wei T. The inhibition of migration and invasion of cancer cells by graphene via the impairment of mitochondrial respiration. *Biomaterials***35** 1597–1607 (2014).

[62] Duch M.C, Budinger G.R.S, Liang Y.T, Soberanes S, Urich D, Chiarella S.E, Campochiaro L.A, Gonzalez A, Chandel N.S, Hersam M.C, Mutlu G.M. Minimizing oxidation and stable nanoscale dispersion improves the biocompatibility of graphene in the lung. *Nano Lett.***11**, 5201–5207 (2011).

[63] Peixoto CA, de Oliveira WH, da Racho Araújo SM, Santana Nunes AK. AMPK activation: Role in the signaling pathways of neuroinflammation and neurodegeneration. *Experimental Neurology***298**, 31–41 (2017).

[64] Milkevitch M, *et al.* Increases in NMR-visible lipid and glycerophosphocholine during phenylbutyrate-induced apoptosis in human prostate cancer cells. *Biochimica et Biophysica Acta - Molecular and Cell Biology of Lipids***1734**, 1-12 (2005).

- [65] Jong CJ, Azuma J, Schaffer S. Mechanism underlying the antioxidant activity of taurine: prevention of mitochondrial oxidant production. *Amino Acids*. **42**, 2223-2232 (2012).
- [66] Schaffer SW, Jong CJ, KC, R, Azuma J. Physiological roles of taurine in heart and muscle. *J. Biomed. Sci.* **17**(Suppl 1):S2 (2010).
- [67] Connolly GP, Duley JA. Uridine and its nucleotides: biological actions, therapeutic potentials. *Trends Pharmacol Sci.* **20**, 218-225 (1999).

Figure captions

Figure 1. Characterization of pegylated nGO sheets. (A) AFM topographic image of dispersed nGO sheets. The graph represents the thickness profile obtained from the white line of the AFM image. (B) nGO sheets particle size distribution obtained by DLS. (C) C1s XPS spectra obtained from nGO sheets.

Figure 2. Cell uptake of pegylated nGO sheets by human Saos-2 cells. (A) Fluorescence profiles of Saos-2 osteoblasts cultured for 24h with nGO (Saos + nGO) compared to control cells in absence of nanomaterial (Saos), quenching the exterior cell surface fluorescence with trypan blue. Morphology evaluation by confocal microscopy of cultured human Saos-2 cells after 24h of treatment without (B) and with (C) nGO sheets. Cells were stained with DAPI for the visualization of the cell nuclei in blue and rhodamine-phalloidin for the visualization of cytoplasmic F-actin filaments in red.

Figure 3. Effect of pegylated nGO sheets on the viability percentage (A) and proliferation (B) of human Saos-2 osteosarcoma cells after 24h of treatment. Statistical significance $*p < 0.05$

Figure 4. 500 MHz HRMAS ^1H NMR spectrum of human Saos-2 osteosarcoma cells, with some assigned metabolites indicated. AMP: adenosine monophosphate, BCAA: branched chain amino acids (valine, leucine and isoleucine), Cr: creatine, Glu: glutamate, GSH: glutathione, Lac: lactate, m-Ino: myo-inositol, PC: phosphocholine, PCr: phosphocreatine, Phe: phenylalanine, Tau: taurine, Thr: threonine, Tyr: tyrosine, UDP: uridine diphosphate.

Figure 5. Multivariate analysis of human Saos-2 osteosarcoma cells spectra. **(A)**PCA scores plot, **(B)** PLS-DA scores plot **(C)** PLS-DA LV2 loadings: Ct vs. nGO. **(D)**PLS-DA LV1 loadings: nGO vs. nGO + laser.

Figure 6. Heatmap of main metabolic variations after nGO incorporation by human Saos-2 osteoblasts (nGO vs. Ct) and after NIR laser irradiation at 1.5 W/cm² power during 5 min (nGO+Laser vs. nGO). Statistical significance ** $p < 0.01$.

Figure 1

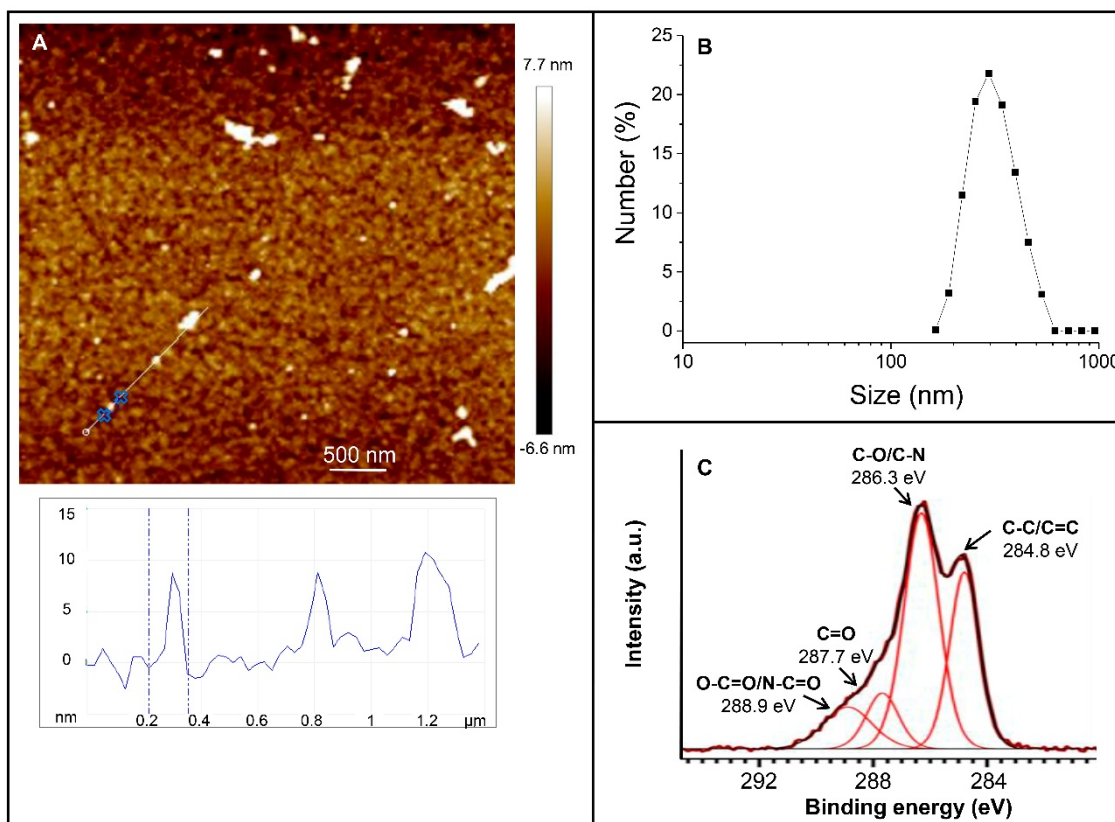


Figure 2

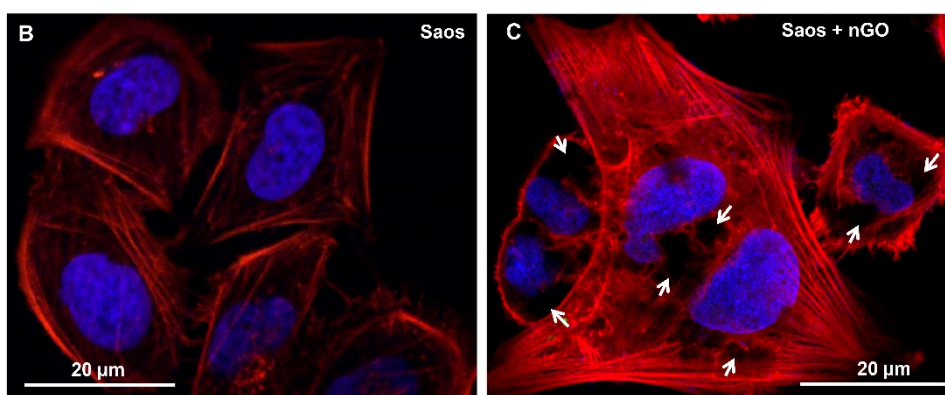
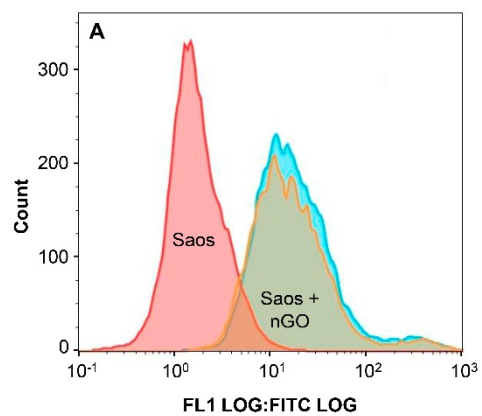


Figure 3

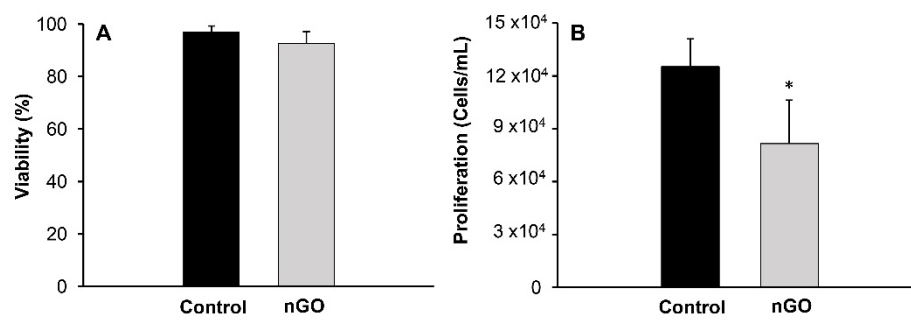


Figure 4

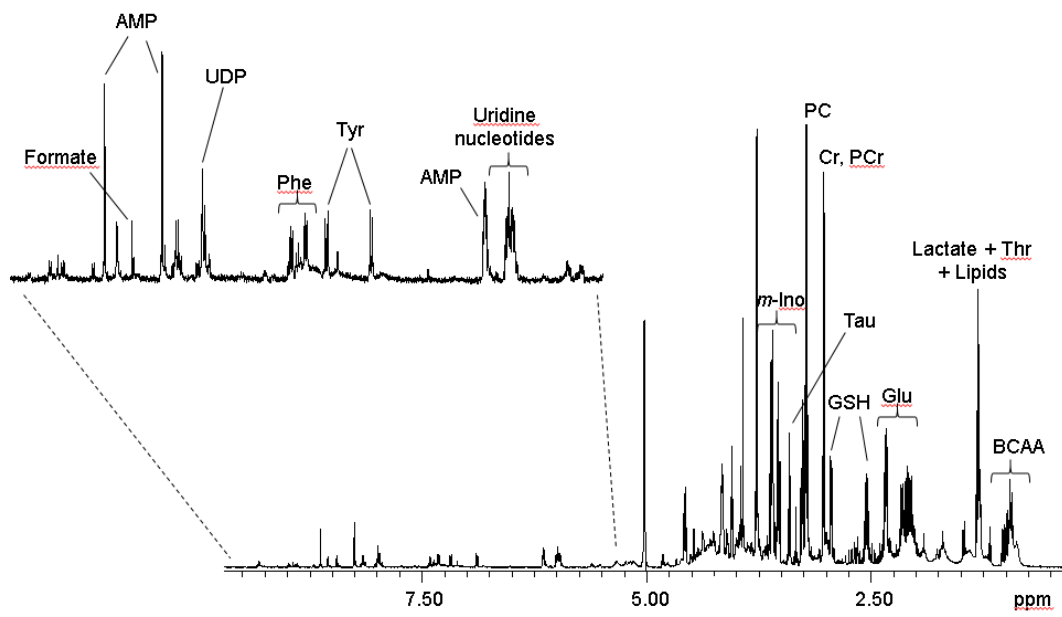


Figure 5

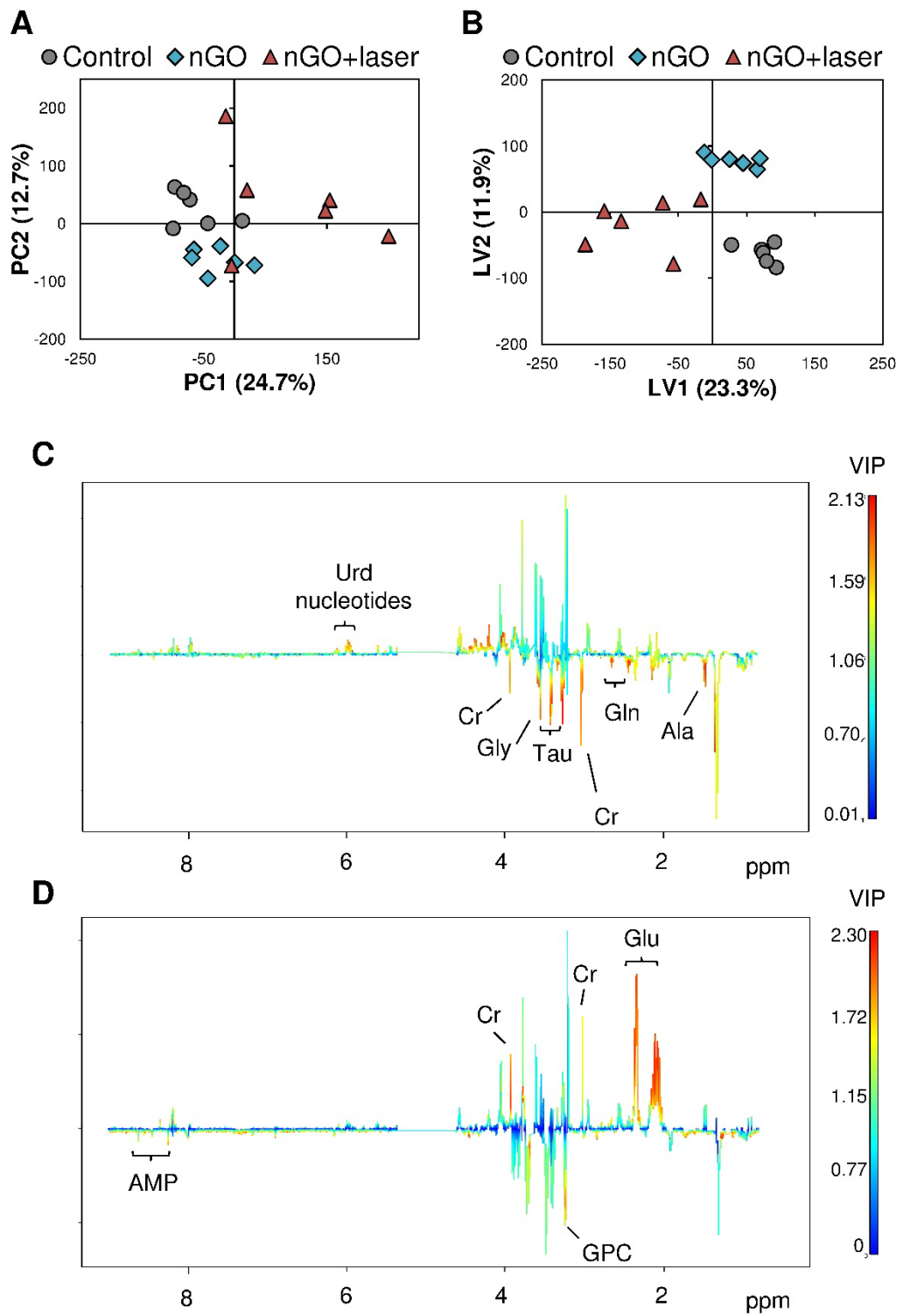
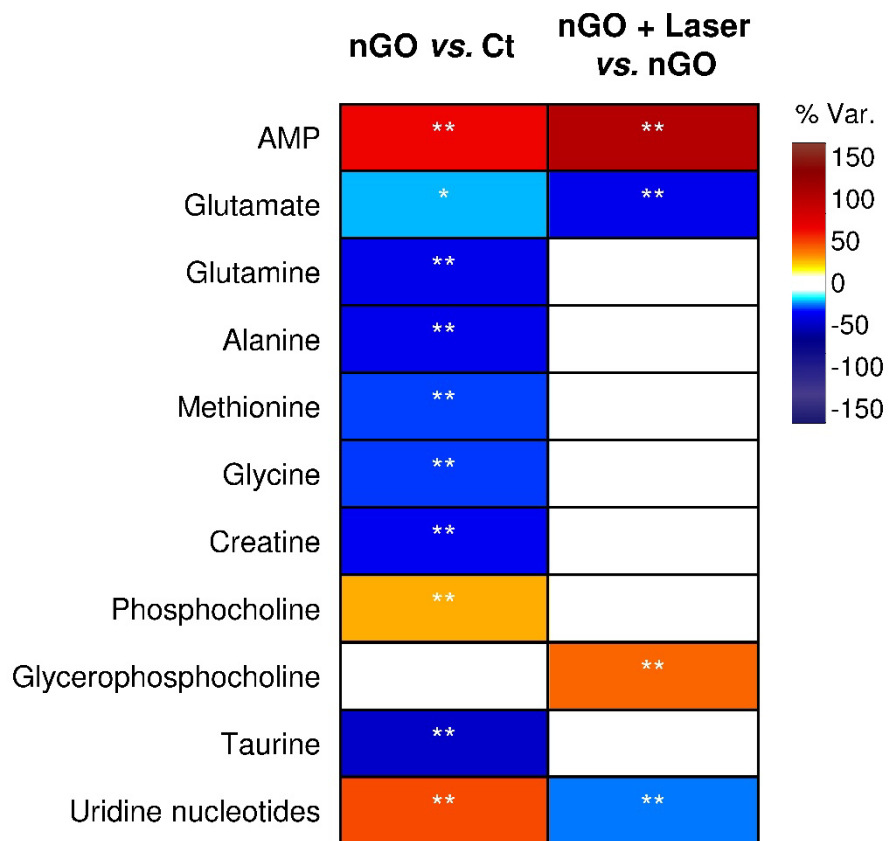
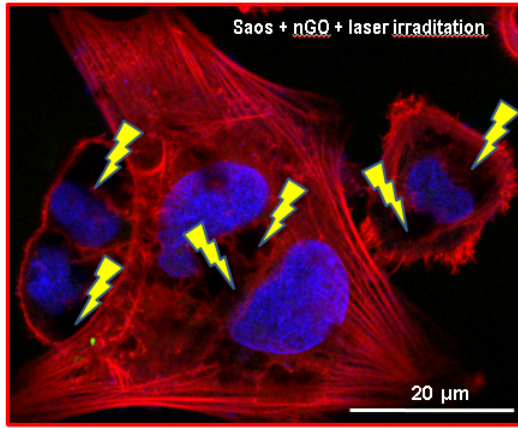


Figure 6



Graphical Abstract



NMR metabolomics

	<u>nGO vs. Ct</u>	<u>Laser vs. nGO</u>	% Var.
AMP	**	**	150
Glutamate	*	**	100
Glutamine	**		50
Alanine	**		0
Methionine	**		-50
Glycine	**		-100
Creatine	**		-150
Phosphocholine	**		
Glycerophosphocholine		**	
Taurine	**		
Uridine nucleotides	**	**	